THE PENNSYLVANIA STATE UNIVERSITY
SCHREYER HONORS COLLEGE

DEPARTMENT OF CHEMISTRY

SYNTHESIS OF MAGNETITE-DERIVED ZERO VALENT NANOIRON AND TARGETING OF ZERO VALENT IRON FOR APPLICATION IN ENVIRONMENTAL REMEDIATION

DANIEL EDWARD FOWLER
Spring 2010

A thesis
submitted in partial fulfillment
of the requirements
for a baccalaureate degree
in Chemistry
with honors in Chemistry

Reviewed and approved* by the following:

Thomas E. Mallouk
DuPont Professor of Materials Chemistry and Physics
Thesis Supervisor

Przemyslaw (Pshemak) Maslak
Associate Professor of Chemistry
Honors Adviser

Raymond E. Schaak
Associate Professor of Chemistry
Faculty Reader

* Signatures are on file in the Schreyer Honors College.

ABSTRACT

Dense non-aqueous phase liquids (DNAPLs) form underground contamination zones that are vast and heterogeneous in their spatial distribution, making them both difficult and costly to remediate. The use of nanoscale zero valent iron (NZVI) as an in-situ agent is a good method for reducing contaminants to less toxic forms, but it is limited by cost, scalability, and hazardous synthetic routes. A new inexpensive and environmentally benign synthetic technique of making carbon-adsorbed NZVI from the reduction of iron oxide (magnetite) with carbon black was developed. Powder X-ray diffraction and scanning electron microscopy confirmed that charged polyelectrolytes were necessary to promote sufficiently intimate mixing of the reactants for production of NZVI. Transmission electron microscopy revealed iron particles on the order of 50 to 150 nm diameter. Delivery of nanoparticles to subterranean contamination zones was modeled by the transport of carbonyl iron powder suspended in anionic polymer solutions through sand columns. Iron particles modified with different anionic polymers were found to target dichlorobenzene-coated sand grains with different degrees of effectiveness. Trends in targeting correlated well with the surface energies of the polymer-modified iron surfaces, which were measured by the contact angle method. The experimental results indicate that NZVI can be produced in a new inexpensive, green manner and that the contaminant targeting properties of micron-sized iron particles can be effectively tailored using simple polymeric adsorbents.

TABLE OF CONTENTS

TABLES AND FIGURES

CHAPTER I

Synthesis and Characterization of Magnetite-Derived Nanoiron

Introduction

As soil and groundwater pollutants continue to threaten human and environmental health[1], a strong need to clean up—or remediate—these contamination zones has arisen. Some of the most threatening are dense non-aqueous phase liquids (DNAPLs), such as chlorinated organic compounds, which persist in subsurface contamination zones for decades.[2] Numerous methods have previously been employed for contaminant removal, including pump-and-treat, solvent flushing, steam treatment, bioremediation, and phytoremediation, each of which possesses drawbacks.[3-7] For certain kinds of sites and contaminants, remediation using nanoscale, zero valent iron (NZVI) has demonstrated significant advantage over other remediation techniques.[3-7] NZVI readily reacts *in situ* (or "at the site") with subterranean DNAPLs to yield non-toxic products. NZVI is more effective than other kinds of iron (such as iron filings or microparticles) because its high surface-to-mass ratio imparts an increased reactivity on the particles.[8] A truly resourceful remediation agent, NZVI has demonstrated both the ability to detoxify heavy metal ions[3,9-11] and nitroaromatics[12,13] as well as the potential for increased reactivity by coupling its use with metal catalysts.[13,14]

The use of NZVI as a remediation agent has traditionally been limited by high materials and production costs, which affect the field use of the material, particularly for large scale projects. On the laboratory scale, iron nanoparticles can be made by using borohydrides to reduce iron salts[13], but this is an expensive technique that also liberates large quantities of hydrogen gas. Hydrogen gas can be used to reduce iron oxide nanoparticles thermally[15], a method that is more scalable and less expensive than the borohydride method. However, the cost of the multistep process required to generate the iron oxide precursors and then reduce them in a

batch reactor with the hydrogen remains relatively high. It has recently been shown that physical milling of larger iron particles can produce reactive nanoparticles, and thus one can start with relatively inexpensive micro-iron particles.[16] An alternative, recently developed method has aimed to eliminate the cost barrier preventing large scale NZVI use by thermally reducing soluble iron salts using carbon black. In principle, this new method could make the synthesis of the reactive nanoparticles significantly less expensive and more scalable.[3] This method is not without its drawbacks, however, as soluble iron salts (which are both expensive and produce waste solutions) were previously used to demonstrate the concept of the carbothermal reduction route. These problems may limit the scalability and "green" character of the overall synthesis.[3]

X-ray diffraction experiments performed with the intermediate products of the carbothermal reduction of iron salts showed that the thermal reduction to make the zero valent particles proceeds through a magnetite (Fe_3O_4) intermediate.[3] This suggested that magnetite – an inexpensive, non-toxic solid iron oxide – could be used in place of water-soluble iron salts in the carbothermal synthesis of NZVI. The reaction of magnetite with carbon to produce carbon dioxide (**Equation 1**) or carbon monoxide (**Equation 2**) is attractive as a scalable route to nano-iron because it involves only solid inexpensive reagents and is endothermic. Thus, local overheating of the solid sample is not a concern when performing the reaction at larger scales.

$$Fe_3O_4(s) + 2\ C(s) \rightarrow 3\ Fe(s) + 2\ CO_2(g), \quad \Delta H^o = +\ 330\ kJ \qquad (1)$$

$$Fe_3O_4(s) + 4\ C(s) \rightarrow 3\ Fe(s) + 4\ CO(g), \quad \Delta H^o = +\ 675\ kJ \qquad (2)$$

Presented here is a new, low-cost method for synthesizing NZVI particles using magnetite as a starting material rather than as an intermediate. Synthetic magnetite nanoparticles were reacted with a stoichiometric excess of carbon black, a method adapted from the previously reported carbothermal technique.[3] Magnetite is a naturally occurring iron oxide that can also be

made from inexpensive starting materials, and its synthesis does not involve organic ligands or solvents. The synthetic route and characterization of the magnetite-derived iron nanoparticles are detailed in this chapter.

Procedure

Nanoiron Synthesis

The scaled up synthesis of magnetite nanocrystals was adapted from a previously reported method.[17] A typical synthesis began by mixing $FeCl_2$ (6.892 g, anhydrous, Mallinckrodt) with $FeCl_3$ (17.640 g, anhydrous, EMD) in 500 mL deionized water in a 1:2 molar ratio. An inert gas (Ar or N_2) was bubbled through the mixture to remove dissolved oxygen and prevent premature iron oxidation. The mixture was heated to 80^{o}C with continuous inert gas flow, after which concentrated NH_4Cl (62.5 mL, 14.5 M, EMD) was added drop-wise over 1 h at a rate of 1 mL/min. After stirring for another hour, citric acid (12.5 g, anhydrous, EMD) dissolved in 25 mL deionized, Nanopure water was added, and the mixture was heated to 95^{o}C for 4 h. After cooling to room temperature, the magnetite particles were centrifuged at 35,000 rpm and washed with deionized, Nanopure water over several cycles to remove excess citric acid. Prior to reaction with carbon black, the magnetite nanoparticles were suspended in deionized, Nanopure water at room temperature.

To promote complete mixing of the carbon black and magnetite particles, charged polymers were added to each reactant suspension prior to intermixing. Poly(acrylic acid) (PAA) sodium salt (Toda Kyogo, Ltd., average MW 3,500) was added to the magnetite suspension to yield a solution 5 mg/mL in the negatively charged polymer, while poly(ethylenimine) (PEI) (Aldrich, average MW 750,000) was added to a carbon black suspension, producing a carbon suspension 5 mg/mL in the positively charged polymer. The magnetite suspension contained 4 g

of the nanoparticles in 190 mL deionized, Nanopure water, while the carbon suspension contained roughly 1.25 g of acetylene carbon black in 75 mL deionized, Nanopure water, a >3:1 molar excess of the carbon for the reduction of the iron oxide. Each polymerized suspension was mixed separately on a Thermolyne rotary shaker for 1 h, after which the two suspensions were stirred together overnight on the rotary shaker. Water was removed by rotary evaporation followed by overnight drying under vacuum.

The solid mixture was ground up using a mortar and pestle and transferred to a small alumina crucible into which it fit with minimal headspace. The covered crucible was placed in a box furnace located in a fume hood, which was purged with an inert gas (Ar or N_2) for 1 h prior to heating in order to lower the partial pressure of oxygen in the furnace to approximately 0.1 atm, as measured previously.[3] With continuous inert gas flow the crucible and contents were heated to 800 ^{o}C at a ramp rate of 4.5 ^{o}C/min and held there for 4 h. After heating, the product was cooled under argon to ~400 ^{o}C, after which argon flow was ceased as the product was left to cool to room temperature.

Particle Characterization

X-ray powder diffraction (XRD) was performed using a Phillips X'Pert MPD X-ray diffractometer, using Cu Kα radiation at 40 kV and a step size of 0.03^{o} 2θ at 1.5 s/step. Nitrogen Brunauer-Emmet-Teller (BET) adsorption isotherms were obtained using a Micrometrics ASAP 2010 surface area analyzer. Transmission electron microscope (TEM) images were gathered at the Electron Microscopy Laboratory at the Pennsylvania State University on a JEOL 1200 EX II microscope. Scanning electron microscope (SEM) images and energy dispersive spectroscopy (EDS) data were obtained at the Materials Characterization Laboratory using an FEI Quanta 200 ESEM microscope. Electrokinetic properties of samples were measured using a ZetaPALS zeta

potential analyzer (Brookhaven Instruments Corporation, Holtsville, NY). Electrophoretic mobility was measured as the average of 5 replicate runs, and the Smoluchowski model was used to convert raw electrophoretic mobility data into zeta potential.

Results and Discussion

Nanoiron Particle Characterization

The product of the carbothermal heating of the magnetite nanoparticles was analyzed using X-ray diffractometry (XRD). XRD analysis confirmed that elemental iron was present in the product. **Figure 1** displays the diffraction pattern of the final product, the most intense peaks of which correspond to body-centered cubic (α-phase) iron, indicating a significant presence of zero-valent iron in the final product. A small face-centered cubic iron peak was present at 45^{o} 2θ, indicating that low quantities of the γ-phase of iron were present as well. Though the majority of the product was zero-valent iron, minor proportions of other compounds were present as well. Unreacted magnetite was also identified in the product using XRD analysis, though in much smaller quantities than zero-valent iron, as evidenced by the significantly lower peak intensities. The presence of magnetite in the final product indicates that the iron oxide reagent did not react completely with the carbon black, due either to a carbon black deficiency in the mixture or limited surface contact between the mixed particles. The graphite-like reflections of carbon can also be seen in the diffraction patterns of **Figure 1** as a broad peak centered at 26^{o} 2θ, a phenomenon typical of the carbothermal synthetic technique, while the reflection from the aluminum sample holder is visible at 78^{o} 2θ.[3] Peaks around 41^{o} and 61^{o} 2θ were indicative of the iron oxide FeO that formed in small quantities due to the slight presence of oxygen during the reaction.

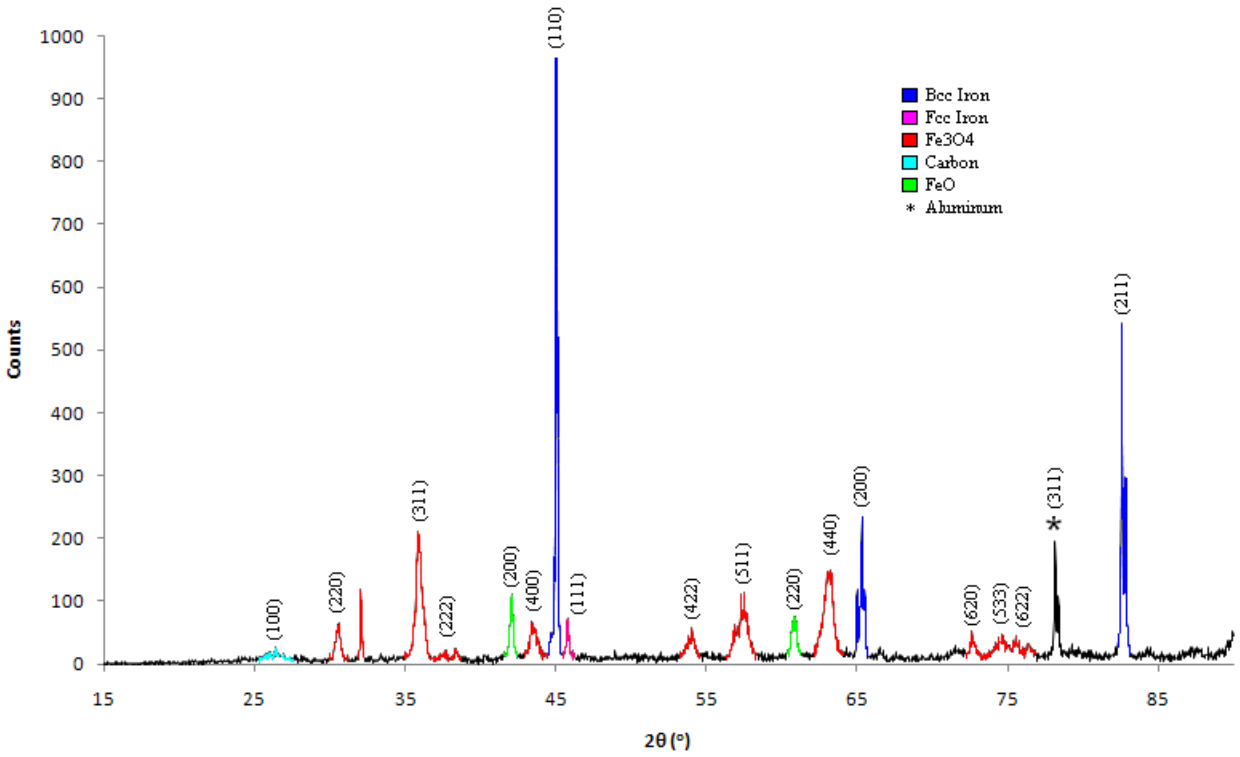

Figure 1: XRD pattern of the carbon black-magnetite mixture after heating. Miller indices are indicated in parenthesis.

C-Fe^0 nanoparticles were further characterized using transmission electron microscopy (TEM). TEM images in **Figure 2** display the nanoiron particles as darker regions adjacent to the lighter carbon regimes. Carbothermal syntheses using iron salts have yielded similarly shaped, roughly spherical nanoiron particles of diameter ~50-150 nm adsorbed to smaller carbon particles.[3] Similarities between nanoparticles derived from the two different methods are due to the magnetite precursor stage common to both techniques. Magnetite forms as an intermediate during heating in the iron salt method[3], compared to its use as a reactant in this technique. Spherically shaped magnetite nanoparticles (**Figure 3**) of diameter ~20 nm were also observed in the product via TEM imaging, a further indication of the presence of unreacted magnetite following heating.

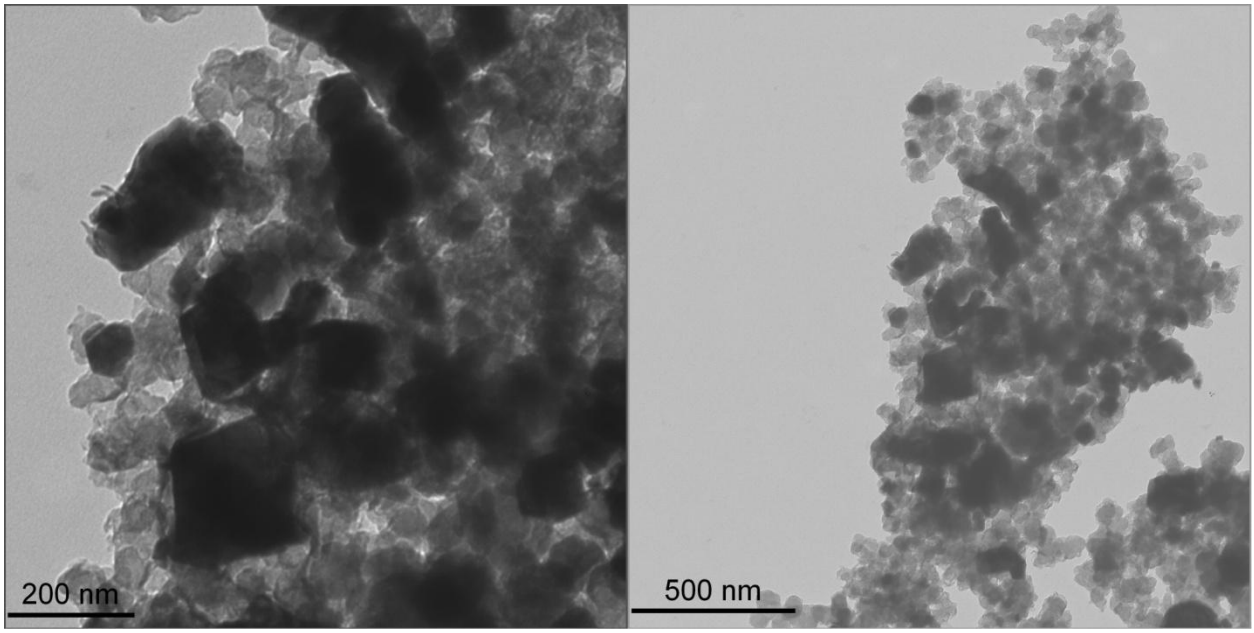

Figure 2: TEM images at different magnifications of C-Fe^0 nanoparticles made from Fe_3O_4

The nitrogen-BET surface area of C-Fe^0 nanoparticles prepared from Fe_3O_4 (13 m^2/g) was lower than surface areas reported using various iron salts, in some cases by an order of magnitude.[3] Previously reported methods similarly observed lower surface areas for C-Fe^0 nanoparticles synthesized via the same impregnation technique used here. The surface area of carbon black was also higher (80 m^2/g), implying that minimal residual carbon remained in the product after heating. Observed above via XRD (**Figure 1**), unreacted Fe_3O_4 remaining in the final C-Fe^0 product also hints at a deficiency of carbon black in the reaction mixture and implies that an even greater excess should be used in future synthetic trials.

Mixing Analysis

Before mixture and subsequent reaction with carbon black, the as-synthesized magnetite nanocrystals were characterized. **Figure 3**, a TEM image of the magnetite particles, demonstrates both the average particle size of 20 nm as well as the tendency of the particles to aggregate. It should be noted that we cannot distinguish by TEM the aggregation that occurs in the suspension from evaporation-induced aggregation on the TEM grid. Aggregation minimizes

interparticle dispersion of magnetite and carbon black during aqueous mixing and ultimately can prevent a successful reaction from taking place between the two reagents. To reduce the degree of aggregation and promote particle mixing, a charged polyelectrolyte was added to the suspension of each reactant. To the magnetite suspension was added the negatively charged PAA, while the positively-charged polymer PEI was added to a carbon black suspension. Enough electrolyte was dissolved in the suspensions to make each 5 mg/mL in polymer concentration, a value previously shown to impart sufficient surface charge on suspended particles.[18]

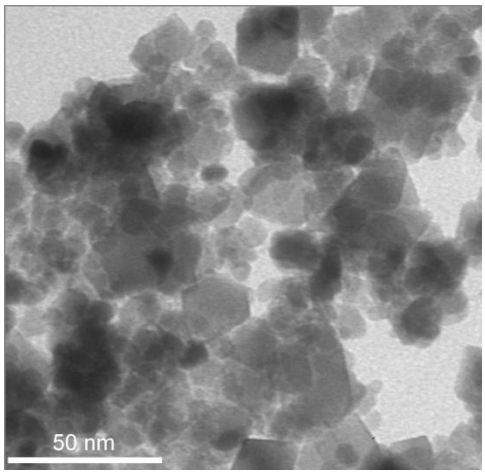

Figure 3: TEM image of magnetite nanocrystals.

Zeta potentials were measured of these as-prepared polyelectrolyte solutions/particle suspensions. The particles were not washed prior to the zeta potential measurements, and the suspensions still contained polyelectrolytes at 5 mg/mL. PAA-treated Fe_3O_4 (pH 7.64) had a zeta potential of -62.54 mV, while PEI-treated carbon black (pH 9.76) had a zeta potential of +56.26 mV, thus confirming that a 5 mg/mL polyelectrolyte concentration successfully imparted opposite surface charges to the magnetite and carbon black particles.

Figure 4 displays SEM images of magnetite nanocrystals and carbon black particles, each prior to mixing with one another and with respective polyelectrolyte adsorbents. Magnetite

nanocrystals of nanometer-scale diameters, which formed massive aggregates (**4a**), were clearly distinguishable from the micron-sized carbon particles (**4b**). The relative range of particle sizes can also be observed by comparing the ~20 nm diameter magnetite crystals in **Figure 3** to the 75 μm diameter carbon particles of **Figure 4b**.

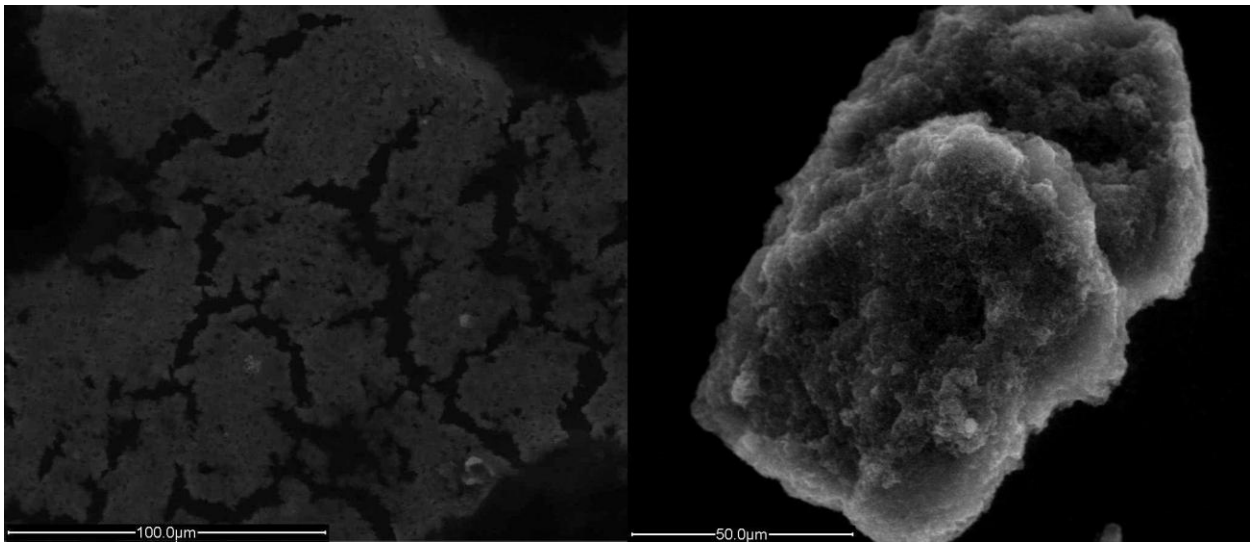

a. **b.**

Figure 4: SEM images of **a.)** magnetite nanocrystals and **b.)** carbon black particles. Images were obtained prior to mixing particles with one another or with respective polyelectrolyte adsorbents.

Figure 5 is a comparison of SEM images of mixed nanoparticles, both with (**5a,c**) and without (**5b,d**) polyelectrolytes added to promote particle interspersion. **Figures 5a,c** and **Figures 5b,d** are clearly different morphologically, with the smaller magnetite nanoparticles adhering to the carbon black particles much more in **Figures 5a,c**. Carbon black particles in the polymer enhanced mixtures (**5a,c**) appear much more heavily coated by iron oxide globules than the carbon particles in the untreated mixtures (**5b,d**).

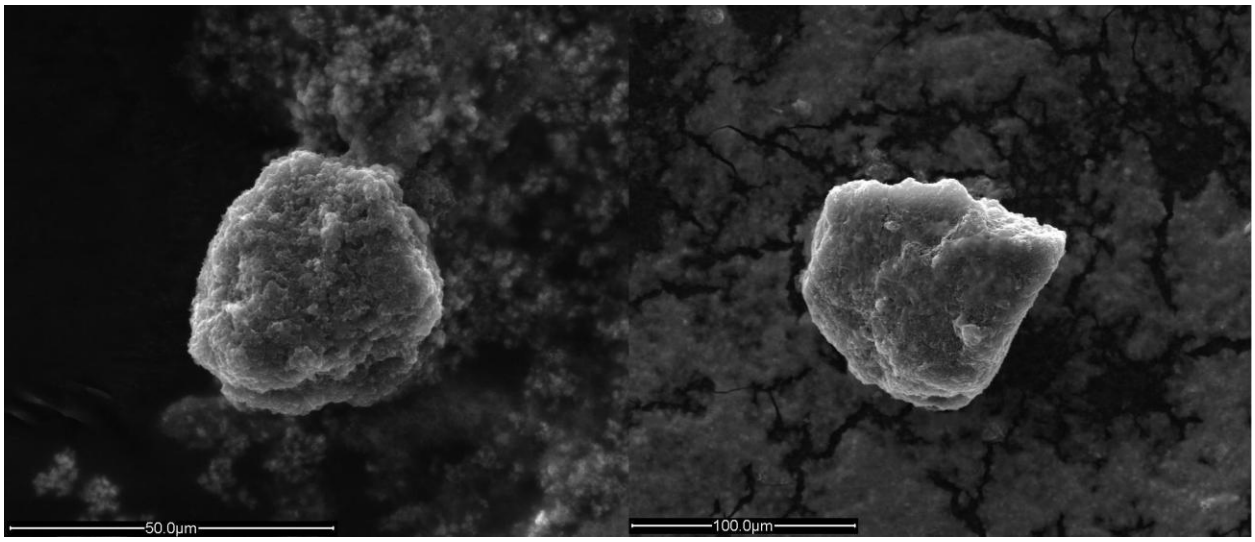

a. **b.**

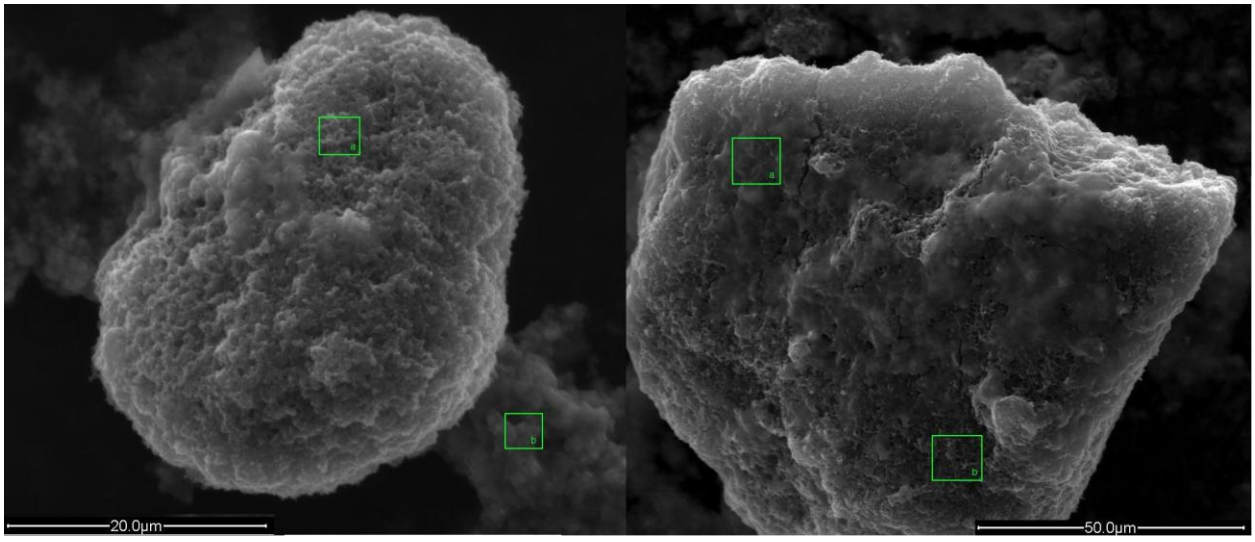

c. **d.**

Figure 5: SEM images before carbothermal reaction of carbon black and magnetite particles mixed together. Images on the left side (**a, c.)** were obtained after suspending the starting materials in solutions of polyelectrolytes PEI (carbon black) and PAA (magnetite) and mixing. Images on the right (**b, d.)** were obtained by mixing particle suspensions without polyelectrolyte treatment. Green boxes indicate regions from which EDS spectra were obtained.

Various carbon black-magnetite mixtures were analyzed both before and after carbothermal heating using energy dispersive X-ray spectroscopy (EDS) (**Table 1**). From the SEM morphology and XRD results, it is evident that the thermal product of the carbon-magnetite mixture that had not been treated with polyelectrolytes did not contain detectable amounts of zero valent iron (**Figure 6**), and this can be attributed largely to the poor extent of mixing, observable in **Figure 5b,d**. In SEM images, the dark spherical carbon particle in **Figure 6a** is coated much more heavily with rounded, light-colored nanoiron particles than the larger carbon particle of **Figure 6b**. While EDS data for the post-heated product confirmed that polyelectrolytes were crucial for successful reactant mixing (and by extension, production of NZVI), the data for the pre-heated mixture were inconclusive (**Table 1**). Some regions sampled on the carbon particle of the polymer-enhanced mixture of **Figure 5c** contained higher percent iron values than the carbon particle of the untreated mixture of **5d**, while other regions contained lower percent iron values. This scatter in the EDS data may reflect the small sampling volume and the inhomogeneous distribution of magnetite on the carbon particles. Further analysis taken over larger sampling areas than those marked by the green boxes of **Figure 5c,d** and **Figure 6** is needed for direct confirmation that oppositely charged polyelectrolytes result in better intermixing of magnetite and carbon black particles.

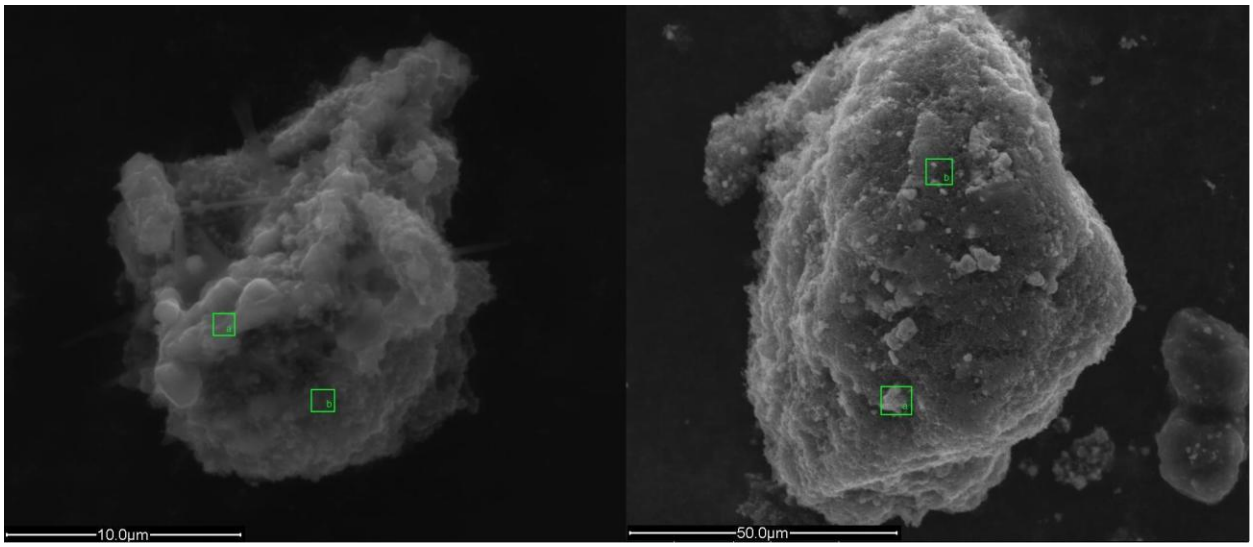

a. **b.**

Figure 6: SEM image of C-Fe^0 nanoparticles **a.)** treated with polyelectrolytes PEI and PAA, respectively after the carbothermal reaction and **b.)** with no prior polyelectrolyte treatment. Green boxes indicate regions from where EDS spectra were obtained.

Table 1: Elemental weight percentages of various carbon-magnetite mixtures as determined by EDS data. Different sampling areas (a, b) for each image are indicated in the table and show substantially different results. The relative error in local compositions obtained by EDS is estimated to be 10-15%.

Pre Heating				
	With Polymer (6c)		No Polymer (6d)	
Element	Weight % - a	Weight % - b	Weight % - a	Weight % - b
C	69	25	60	59
O	17	34	22	9
Fe	14	41	18	32
Post Heating				
	With Polymer (7a)		No Polymer (7b)	
Element	Weight % - a	Weight % - b	Weight % - a	Weight % - b
C	29	65	31	85
O	33	16	9	8
Fe	38	19	60	7

XRD patterns, which sample the entire volume of the composite materials, confirmed that polyelectrolytes were essential for the successful mixing and subsequent generation of C-Fe^0 particles from carbon black and magnetite (**Figures 1,7**). Patterns for the untreated product (**Figure 7**) identified minimal Fe^0 in the product, whereas the most intense peaks for the polyelectrolyte treated product patterns corresponded to body-centered cubic zero valent iron (**Figure 1**). Additionally, no potential products of the decomposition of either polyelectrolyte were identified in the electrolyte treated iron product.[19,20]

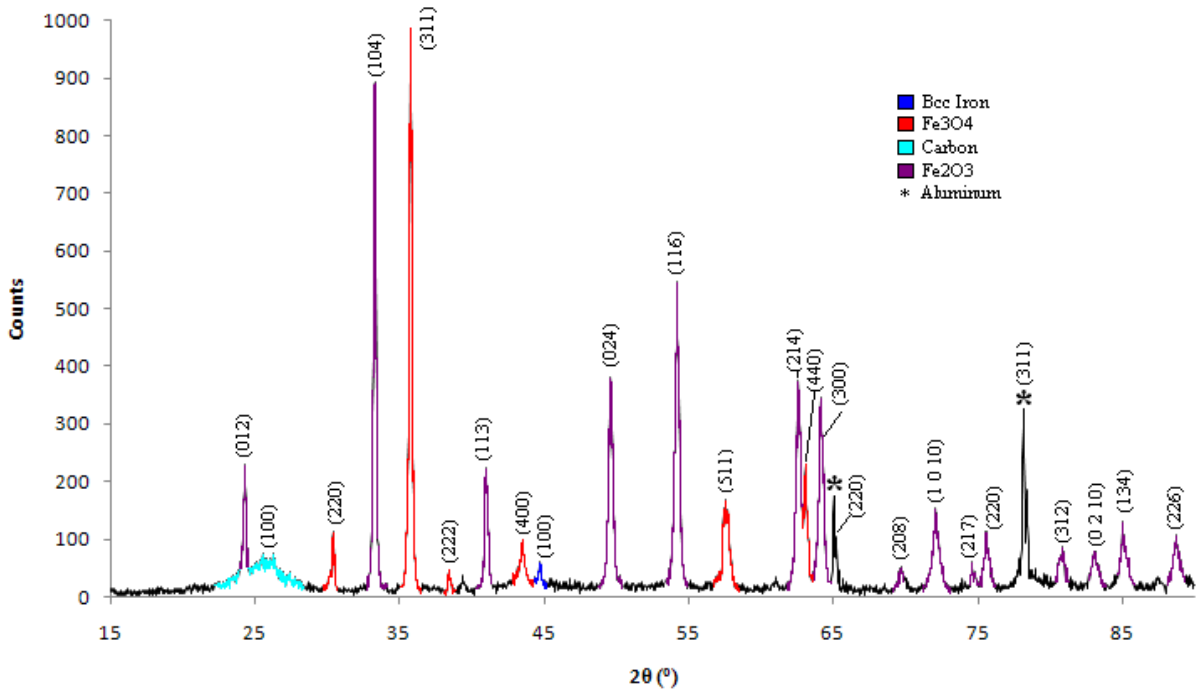

Figure 7: XRD pattern of C-Fe^0 derived from untreated magnetite and carbon black. Miller indices are indicated in parenthesis.

Conclusions

An inexpensive, green method of synthesizing nanoscale zero valent iron was successfully developed via the reduction of magnetite nanoparticles using carbon black. This synthesis represents an improvement over the previously developed carbothermal method, which involved more expensive iron salts and generated some solution waste products. It is not yet known if either method produces toxic gas byproducts such as carbon monoxide in the carbothermal reduction process, and this should be investigated in follow-up studies. Transport and reactivity studies of NZVI made by the carbothermal method from iron salts show good transport characteristics in the presence of anionic polymer dispersants and also good reactivity with Cr(VI).[3] Similar experiments need to be done with the materials made in this study.

One of the most interesting findings in this work was the development of a successful strategy to promote particle mixing in a solid-solid reaction. The synthesis of nano-iron was successful only when the magnetite and carbon precursors were suspended in oppositely charged polyelectrolyte solutions prior to mixing. SEM and XRD analyses demonstrated the importance of charged polyelectrolytes in promoting complete dispersion between magnetite and carbon particles prior to thermal reduction. The carbothermal reaction was done under an atmosphere containing a reduced level of oxygen but did not require additional reactants, such as hydrogen. As an endothermic reaction, this process should be scalable to much larger quantities of NZVI. XRD and TEM analysis confirmed the presence of 50-150 nm-sized iron nanoparticles, though detectable amounts of magnetite nanocrystals remained after reaction, implying a larger stoichiometric excess of carbon may be required for the total conversion to Fe^0.

CHAPTER II

Zero Valent Iron Targeting by Simple Homopolymers

Introduction

Developing an efficient method of delivering NZVI particles to contamination sources in soil and ground water is an important practical problem. DNAPL contamination zones form in the underground environment several different ways, including as hydrophobic liquid droplets—known as "ganglia"—that slowly equilibrate with the ground water because of low solubility.[21] High reactivities and poor subterranean transport properties make the efficient delivery of iron nanoparticles to these underground ganglia a particularly difficult problem. Recent studies have shown that nanoscale iron particles are relatively immobile in saturated granular media such as soils, with filtration lengths on the order of a few centimeters. However, particle transport can be improved using microemulsions[22] and a variety of different adsorbents—including anionic polymers[23,24], anionic carbons[3,23], silica[25], and triblock copolymers[24,26]—as particle "delivery vehicles." Of these techniques, it has been shown that anionic polymers impede particle aggregation and result in lower values for sticking coefficients, or the probability that collisions between the particles and soil surfaces result in adhesion.[18,27]

Lowry and coworkers introduced the concept of targeting nanoparticles to contaminants in their studies of triblock copolymer layers adsorbed to iron nanoparticles. They found that particles coated with triblock copolymers localized to the liquid-liquid interface between water and liquid trichloroethylene.[24] They attributed this behavior to the triblock copolymer's ability to rearrange in different environments, specifically to expose the hydrophobic polystyrene block when in contact with DNAPLs. However, earlier studies have shown that, in general, particles tend to localize at liquid-liquid interfaces when the two contacting liquids have a much higher surface tension ($\gamma_{L1,L2}$) than that of the two particle-liquid interfaces ($|\gamma_{p,L1}-\gamma_{p,L2}|$).[28] As a high

surface tension is expected for DNAPL-water interfaces, moderately hydrophobic polymer coatings should lower the particle-liquid surface tension enough to cause particles to localize preferentially at the interface between water and DNAPL ganglia. From the point of view of efficiency of DNAPL remediation, such targeting would be highly desirable for in situ remediation applications.

This chapter describes a method for observing and quantifying the partitioning of iron particles between unmodified (hydrophilic) and dichlorobenzene-modified sand grains, in transport experiments that model the flow of iron particle suspensions through contaminated soil. Micrometer-sized carbonyl iron powder (CIP, an industrial iron standard made from the decomposition of iron pentacarbonyl[29]) particles were chosen to model remediation iron's transport because of their spherical shape and lower reactivity, properties which impart on the particles better adherence to classical filtration theory (CFT) models than their nanometer-sized counterparts.[18] This method allows one to calculate particle sticking coefficients from particle elution data within the framework of CFT models. Previous studies have shown that CFT, which cannot be rigorously applied to "real world" particle elution experiments, is an adequate model under the conditions used in this work.[18] The partitioning behavior of particles modified with several anionic homopolymers was correlated with particle surface energies, which were measured by the contact angle method. This correlation is useful for selecting anionic polymers that "target" iron efficiently to contaminants, i.e. those that impart a low sticking coefficient for polar, unmodified sand grains but a high sticking coefficient for DNAPL surfaces.

Procedure

Materials

Ottawa sand (160 ± 45 μm diameter, 0.01% organic matter) was available from a previous study.[18] Hexadecyltrimethoxysilane (HTMS) was obtained from Gelest. *Ortho*-dichlorobenzene (reagent grade) and *para*-dichlorobenzene were obtained from Aldrich. Meso-tetraphenylporphine was obtained from Alfa Aesar. Carbonyl iron powder, CIP-HQ, was obtained from BASF. Polyacrylic acid sodium salt (PAA), average MW 3500, was provided by Toda Kogyo, Ltd. Sodium metasilicate (SMS) (anhydrous, SiO_2 content 45.8-47.3 %), and alginic acid, sodium salt (ALG), were obtained from Aldrich. Carboxymethylcellulose, sodium salt (CMC), MW 200,000-400,000, was obtained from Calbiochem.

Iron Particle Transport Experiments

Hydrophobic sand was made by reacting Ottawa sand with HTMS. Sand (146.8 g) and triethylamine (36.8 g) were stirred in 318.6 mL (367.5 g) of toluene, followed by the addition of 11.8 mL HTMS. After the reaction, the liquid was decanted off and the sand was washed twice with acetone and filtered in vacuo. The sand was then dried at 120^{o}C. A eutectic mixture of dichlorobenzene isomers was made by combining 13 g of the solid *para* isomer with 10 mL (13 g) of the liquid *ortho* isomer. To prepare sand columns with 5% modified grains, 0.5 mL of this liquid was mixed with 3.75 g hydrophobic sand and (when fluorescent grains were needed) 1.0 mg meso-tetraphenylporphine. This mixture was placed in a freezer at -10^{o}C for 30 min and then ground with a cold mortar and pestle. Unmodified sand (71.25 g), also at -10 ^{o}C, was combined with the frozen mixture and re-ground. The frozen sand/dichlorobenzene mixture was added slowly to a column containing a mixture of 75% water and 25% isopropanol. The loaded column was then warmed to ambient temperature.

Layered columns were loaded with a bottom and top uncontaminated sand layer and a 10% (by mass) contaminated sand grain middle layer. A bottom layer of unmodified (hydrophilic) sand was first added slowly to a column containing a mixture of 75% water and 25% isopropanol, as described above. Atop this unmodified layer was next added the 10% contaminated sand layer, prepared as described above, followed by a final third layer of unmodified sand to the top of the column. The three layers were each 30 g in mass and of approximately equal lengths (~20 cm). Prior to the addition of any iron particle suspensions, all of the remaining isopropanol/water mixture was eluted from the column until the solvent line lay just above the sand surface.

Transport experiments were carried out as previously described using glass columns containing roughly 75 g (51.7 cm) of the collector phase.[18] Iron particle stock suspensions were made by mixing carbonyl iron powder with water. The appropriate polymer was then added, followed by thorough mixing. In each experiment, the stock suspension contained 5.0 ± 0.5 mg iron and 2.0 mg of polymer per mL of deionized water. Nanopure water, resistivity 18.2 MΩ-cm, was used to make all solutions/suspensions. The particle suspensions, which settled rapidly, were shaken just before injection into the columns. In a typical column trial, a pure polymer adsorbent solution (2 mg/mL, 125 mL) was introduced at the top of the column. A few milliliters of solution were first added slowly via pipette to preserve the flat sand surface, after which the solution was poured directly into the column. Each solution was allowed to elute at an approximate flow rate of 18 mL/min, corresponding to a linear velocity of 0.152 cm/s in 42% porosity columns. In almost all cases, this could be accomplished by simple gravity flow by adjusting the stopcock at the bottom if the column. In the case of CMC, however, air pressure was applied at the top of the column in order to maintain the flow rate at 18 mL/min. Without

changing the flow rate of the column, an iron suspension (2 mg/mL polymer, 5 mg/mL iron, 400 mL) was added. A second polymer solution (2 mg/mL, 125 mL) was added on top of the suspension in order to elute unretained iron.

Iron retained in different column layers was measured by taking cuts of the top (uncontaminated) and middle 10 % contaminated layers and analyzing using a previously developed colorimetric method.[30] Taking a cut consisted of connecting the bottom of the column to tubing and applying a light air flow, slowly forcing the wet sand out of the column while preserving the column's shape, followed by removal of equal masses of the sand from immediately above and below the border between the two topmost layers. Wet samples (~20 g, each containing about 10 g of dry sand) were separately treated with HCl (5 mL, 6.0 M) to dissolve the iron, hydroxylamine HCl (0.5 mL, 1.5 M) to reduce dissolved iron to Fe^{+2}, sodium acetate buffer (5 mL, 1.2 M) to preserve the sample pH, and *ortho*-phenanthroline (5 mL, 1 mg/mL) to complex the ferrous ions. Samples were shaken using a vortex mixture and left to sit overnight to ensure the maximum amount of iron dissolved and complexed. Clean, unmodified sand wet with Nanopure water equal in mass to the column cuts (~20 g) was treated identically with HCl, hydroxylamine HCl, sodium acetate, and phenanthroline and also left to sit overnight. Absorbances of sample solutions were measured at 508 nm using this blank sand solution as a reference. A previously generated calibration curve for Fe^{+2} concentration was used to calculate the mass and percent of iron present in the samples.

Contact Angle Measurements

Samples for contact angle measurements were prepared using a method previously developed for powder samples.[31] An adhesive (3M Spray Mount Adhesive) was applied to a glass slide and allowed to dry for 30 s. The slide was placed in a container of iron powder (CIP-

HQ) and shaken vigorously for 1 min to completely cover the adhesive. Excess iron powder was removed by tapping and then wiping the slide clean. Iron sample slides were immersed several times for 5 s each in either nanopure water or 5 mg/mL aqueous solutions of PAA, CMC, ALG, or SMS, and then air dried for several minutes.

Static contact angles of water, ethylene glycol, and formamide on the iron-coated slides were measured using a contact angle goniometer. Ethylene glycol (reagent grade) and formamide (puriss grade) were obtained from J.T. Baker and Riedel-de Haën, respectively. Images were captured using the Measurement & Automation Explorer program (National Instruments, Version 4.1.3001) and were analyzed to compute contact angles using ImageJ software (Version 1.37a).

Results and Discussion

Iron Targeting Behavior

The approach taken to observe and quantify targeting of iron particles to contaminants involves analysis of the elution behavior of micron-size iron particles in lightly contaminated water-saturated sand columns. Quantitative transport models generally assume a single collector size and a uniform pore velocity. In order to maintain a single collector diameter, sand particles 160 ± 45 μm in diameter were modified with a hydrophobic silane monolayer to which a thin (~10 μm) coating of dichlorobenzene was applied. The modified grains were then dispersed at 5-10% mass loading in unmodified sand. By using a mixture of dichlorobenzene isomers that was solid at the mixing temperature (-10^{o}C), it was possible to prevent agglomeration of the dichlorobenzene-coated grains. **Figure 8** shows an optical microscope image of a 5% sand grain mixture in both bright field and fluorescence modes. The image illustrates that the modified and unmodified sand grains are similar in size and that the former are well dispersed in the latter.

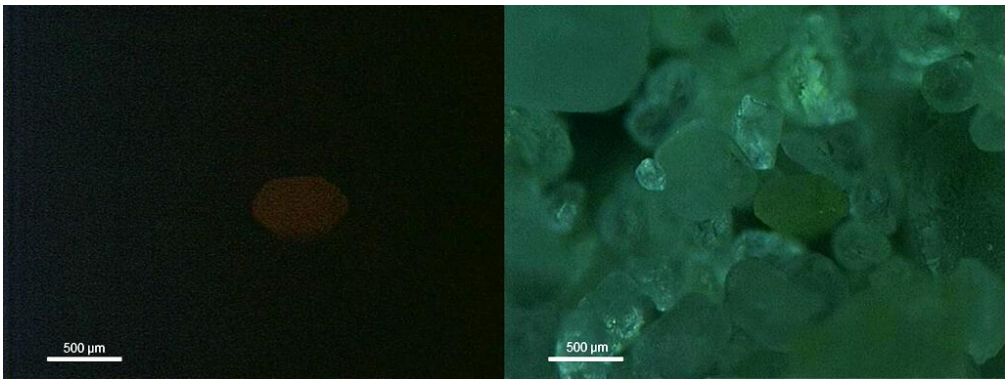

Figure 8: Optical microscope images of a sand mixture containing 95% sand and 5% dichlorobenzene-coated sand grains. The dichlorobenzene layer was stained with fluorescent meso-tetraphenylporphine. Left: bright field image. Right: fluorescence image.

Earlier studies of micro-iron transport in sand columns showed that the profile of retained particles along the length of the column deviated somewhat from the exponential decay predicted by CFT.[18] Larger particles are captured at a faster rate (i.e., preferentially at the top of the column), because they are trapped in a secondary energy minimum that is deep relative to the thermal energy.[32] Despite the non-exponential profile of retained iron, the elution can in practice be adequately represented by an average sticking coefficient, and the large values of α_{DNAPL} found for mixed columns (in some cases 30 times higher than α for simple sand columns[30]) cannot be explained by these small deviations from CFT. Microscopic analysis of the particles from mixed columns (**Figure 9**) shows that iron particles are localized strongly to the contaminated grains with certain polyelectrolytes.

Sand columns were prepared with layers of uncontaminated and contaminated sand in order to visualize the preferential capture of polymer-modified iron particles by the contaminated layers. **Figures 11-13** show the contrast in the amount of retained iron for different polymers, two of which (CMC and PSS) are sufficiently hydrophobic to promote targeting (**Figure 10**).

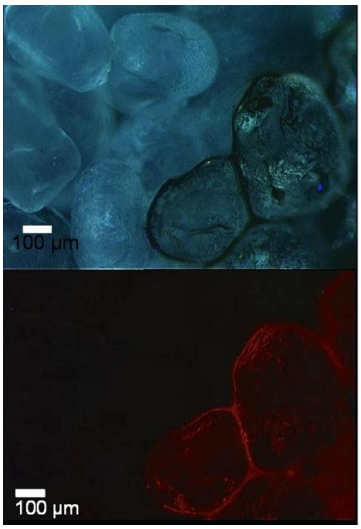

Figure 9: Bright field and fluorescence image of sand particles obtained from contaminated columns eluted with iron/CMC suspensions. In this image, iron particles coat the contaminated grains containing the porphyrin fluorescent marker but not the unmodified sand grains.

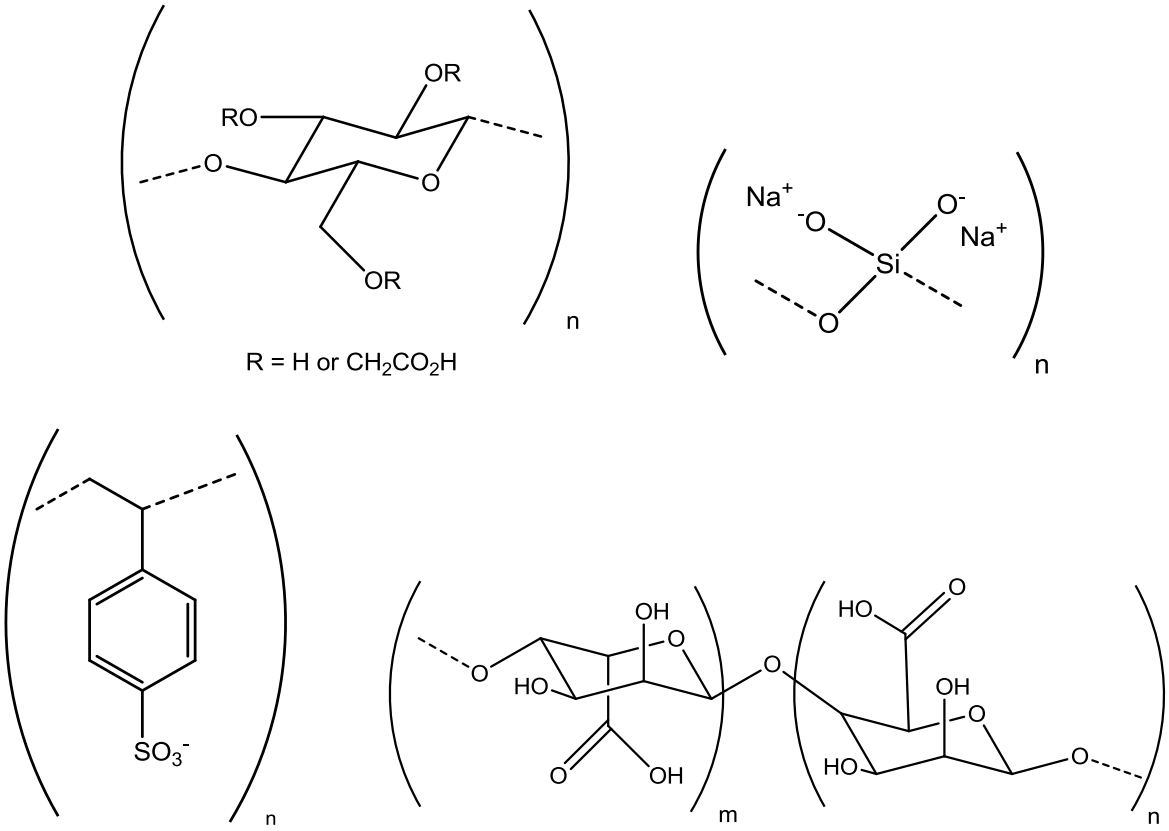

Figure 10: Polymeric backbone structures of carboxymethylcellulose (CMC, top left), sodium metasilicate (SMS, top right), poly(styrene sulfonate) (PSS, bottom left), and alginic acid (ALG, bottom right).

In these cases, the difference in sticking coefficient between the sand and contaminant were so large that differences in iron retention were noticeable by eye. With CMC, elution experiments with mixed sand/contaminant columns gave a ratio of sticking coefficients of about 30,[33] and a strong contrast between the two layers is visually observed (**Figure 11**). With PSS, the column elution results were ambiguous, but again the contrast between the contaminated and pure sand layers is clear (**Figure 12**). On the other hand, the more polar SMS polymer, which does not

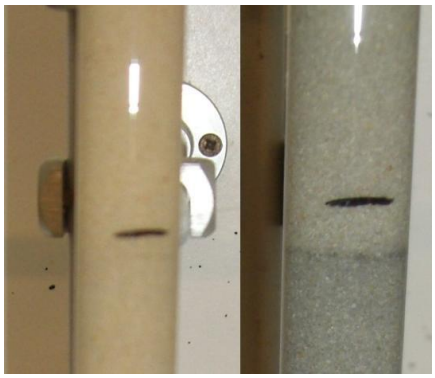

Figure 11: Sand columns before (left) and after (right) elution with the CMC-adsorbed iron suspension. Settling of the sand occurs from washing with the solutions; hence, the layer marked by the black line on the left moves below the black line (right) following elution.

Figure 12: Sand columns before (left) and after (right) elution with the PSS-adsorbed iron suspension. Slight settling of the sand can be observed in the right image.

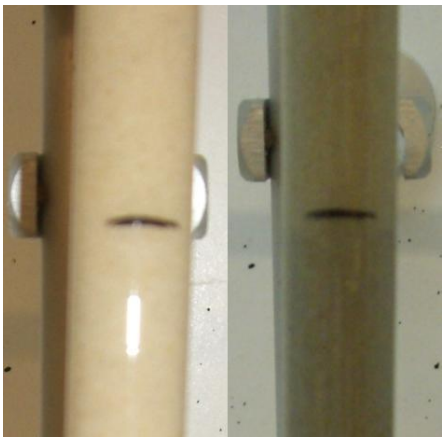

Figure 13: Sand columns before (left) and after (right) elution with the SMS-adsorbed iron suspension. Settling of the sand due to washing can again be observed in the right image.

show preferential targeting of contaminants in the eluted iron experiment, does not show a significant contrast between layers (**Figure 13**).

Specifically calculated amounts of iron in CMC, SMS, and PSS tri-layered columns can be found in **Table 2**. Results for each individual polymer are largely consistent with previous findings[33]; that is, CMC imparted a significant increase in the amount of iron retained in the contaminated layer versus the uncontaminated layer while SMS had little effect. Analytical data for PSS was ambiguous, as the polymer seemed to decrease the amount of iron retained in the contaminated layer (**Table 2**), contradicting visual observations that suggest more iron in the contaminated layer (**Figure 13**). Differences in amounts of retained iron in both layers also reflected different α_{sand} values for the different polymers. Although CMC targeted the contaminated layer effectively, both layers were relatively low in iron (compared to the SMS and PSS cases) because of the lower α_{sand} value for CMC.

Table 2: Amounts of iron found in different sand column layers after elution with various polymer-adsorbed iron suspensions.

Polymer	Absorbance at 508 nm	Iron Concentration (10^{-3} mg/mL)	Percent Iron by Mass (10^{-4} %)
CMC			
Uncontaminated Layer	0.0212	0.0106	0.185
10% Contaminated Layer	0.301	1.22	2.11
SMS			
Uncontaminated Layer	0.456	1.89	3.09
10% Contaminated Layer	0.606	2.53	4.15
PSS			
Uncontaminated Layer	0.546	2.27	3.23
10% Contaminated Layer	0.350	1.43	2.04

Surface Energy-Targeting Behavior Correlation

The surface energy (γ) of iron microparticles with adsorbed polymer layers was estimated from contact angle data. Samples were prepared using a method previously developed for contact angle measurements of pharmaceutical powders.[31] A clean glass slide was sprayed with an adhesive and allowed to dry for several seconds. Iron powder was applied to the adhesive, after which the slide was immersed in a 5 mg/mL polymer solution to adsorb the polymer to the surface. Static contact angles were measured with three polar fluids—water, ethylene glycol, and formamide—using a contact angle goniometer. Attempts to measure contact angles with less polar fluids were unsuccessful because those solvents swelled or dissolved the adhesive. In a typical measurement, a drop of liquid was deposited on the surface of the iron-coated slide, and a static contact angle image was captured. Between 9 and 15 images were obtained for each measurements and the results were averaged. The standard deviation of the mean was taken as the uncertainty in the calculations.

The surface tension of each iron surface was calculated using equation (3).[34]

$$\gamma_L(1+\cos\theta_{SL}) = 2(\sqrt{\gamma_S^{\,d}\gamma_L^{\,d}} + \sqrt{\gamma_S^{\,p}\gamma_L^{\,p}} + \sqrt{\gamma_S^{\,h}\gamma_L^{\,h}}) \quad (3)$$

Here γ_L is the liquid surface tension; γ_L^d, γ_L^p, γ_L^h are the liquid surface tension components due to dispersion, polar, and hydrogen-bonding forces, respectively; θ_{SL} is the contact angle of the liquid with the solid surface; and γ_S^d, γ_S^p, γ_S^h are the solid surface tension components due to dispersion, polar, and hydrogen-bonding forces, respectively. Because contact angles were measured for three different liquids, three equations are generated:

$$\gamma_{L,water}(1+\cos\theta_{SL,water}) = 2(\sqrt{\gamma_S^{\,d}\gamma_{L,water}^{\,d}} + \sqrt{\gamma_S^{\,p}\gamma_{L,water}^{\,p}} + \sqrt{\gamma_S^{\,h}\gamma_{L,water}^{\,h}}) \quad (4)$$

$$\gamma_{L,glycol}(1+\cos\theta_{SL,glycol}) = 2(\sqrt{\gamma_S^{\,d}\gamma_{L,glycol}^{\,d}} + \sqrt{\gamma_S^{\,p}\gamma_{L,glycol}^{\,p}} + \sqrt{\gamma_S^{\,h}\gamma_{L,glycol}^{\,h}}) \quad (5)$$

$$\gamma_{L,form}(1+\cos\theta_{SL,form}) = 2(\sqrt{\gamma_S^{\,d}\gamma_{L,form}^{\,d}} + \sqrt{\gamma_S^{\,p}\gamma_{L,form}^{\,p}} + \sqrt{\gamma_S^{\,h}\gamma_{L,form}^{\,h}}) \quad (6)$$

For each polymer-coated iron surface, contact angles of the three liquids were measured, providing the θ terms on the left side of equations (4-6) for the sample. The total surface tension and component values have been previously reported for each of the three liquids, and thus each of the γ_L terms is known.[35] This gives for each surface three equations in three unknowns ($\sqrt{\gamma_S^{\,d}}$, $\sqrt{\gamma_S^{\,p}}$, and $\sqrt{\gamma_S^{\,h}}$), which can be solved to calculate the solid surface tension components of the polymer-coated iron particles. The values obtained were squared to give γ_S^d, γ_S^p, and γ_S^h, respectively. These components were then summed to obtain the total solid powder surface tension γ_S for a given iron particle surface (**Table 3**). In the case of the polar polymers (SMS and ALG, see **Figure 10** for structures), contact angles were too low to measure with polar fluids, i.e., the drops spread completely on the surface. It is important to note that the

unmodified iron powder sample used as a control sample gave measurable contact angles with these fluids. Thus one can conclude that the wetting observed with SMS and ALG is a result of polymer adsorption on the surface.

The surface energies calculated for SMS- and ALG-coated surfaces are rough estimates, obtained by using 0 values for contact angles where indicated in **Table 3**. One can conclude nevertheless that these are high energy surfaces that are completely wetted by water (γ_{water} = 78.3 mN/m) and formamide. In contrast, the PAA- and CMC-coated iron surfaces gave significantly lower total surface energies.

Table 3: Contact angle data and calculated surface energies of polymer-coated iron particles.

	PAA	**CMC**	**SMS**	**ALG**	**Unmodified Iron**
Contact Angle θ - Water (^{o})	63.9±1.6	50.7±5.3	0 (too low to measure)	0 (too low to measure)	30.3±2.3
Contact Angle θ - Ethylene Glycol (^{o})	55.5±1.7	43.9±3.6	11.2±1.0	0 (too low to measure)	18.8±1.7
Contact Angle θ - Formamide (^{o})	40.8±2.9	33.3±3.4	0 (too low to measure)	0 (too low to measure	38.3±2.5
γ_s^d (mN/m)	12.7±0.9	5.0±0.9	0 (estimate)	0 (estimate)	0.1± 0.0
γ_s^p (mN/m)	10.0±0.8	33.7±2.4	43.4 (estimate)	41.5 (estimate)	24.2±0.8
γ_s^h (mN/m)	16.3±1.0	14.7±1.6	42.3 (estimate)	42.7 (estimate)	47.4±1.1
γ_s^{tot} (mN/m)	39.0±2.6	53.4±5.0	85.6 (estimate)	84.2 (estimate)	71.6±2.0

For the anionic homopolymers studied here, there is a strong correlation between particle surface energy (**Table 3**) and iron partitioning behavior, both from this study (**Figures 11-13, Table 2**) and from corresponding elution data on mixed sand columns.[36] Polymers that gave low

water contact angles (SMS, ALG) did not result in DNAPL targeting, whereas the more hydrophobic polymers (PAA, CMC) registered much higher concentrations of iron in contaminated layers than in uncontaminated layers, observable both optically and spectrophotometrically. This correlation implies that the best polymer adsorbates for the *in situ* remediation of DNAPLs by iron particles should be moderately hydrophobic.

Calculations of the sticking coefficients (α), or soil adhesion probabilities, for microscale iron eluted through mixed (sand + contaminated sand) columns are also consistent with these results and correlation.[36] These calculations are based on CFT, which has previously been shown to represent accurately the profile of retained micro-iron in sand columns at sufficiently slow flow rates ($\leq$ 0.05 cm/s) and, at higher flow rates, for sections of the column that are more than about 5 cm from the top.[18] Slower flow rates should lead to higher particle retention according to CFT,[32] and faster flow rates tend to accentuate the deviation of elution behavior from the simple CFT model, leading to slightly lower average α_{sand} values.[18] Using slower flow rates, it should be possible to calculate accurate α values from analysis of retained iron in the contaminated and uncontaminated parts of the column. Since the data presented here were obtained at a linear flow rate of 0.152 cm/s and since there was not a sufficient column length above the sampling area, only approximate values could be calculated. Thus, a priority for future experiments will be to obtain quantitative analytical data under conditions that can be accurately modeled by CFT, in order to obtain a more complete picture of DNAPL targeting by polymer-coated iron.

Conclusions

Data from this study on the transport behavior of polymer-adsorbed microscale iron particles confirms that simple anionic homopolymers promote particle targeting of DNAPL contamination zones. Hydrophobic adsorbent polymers (PAA, CMC) effectively targeted CIP to a dichlorobenzene contaminant in multilayered sand columns, an effect observable both visually and colorimetrically, while hydrophilic polymers (SMS, ALG) imparted no effect on targeting. This behavior strongly correlates with surface energy of polymer-modified iron surfaces, measured and calculated from contact angles. Quantification of the targeting phenomenon is also possible but was not studied here for multilayered sand columns because the elution conditions were not ideal for use of CFT. In order to identify the best delivery vehicles for iron nanoparticles, which are more environmentally relevant than the iron microparticles used in these model trials, the methods described here will need to be modified and extended. In particular, iron nanoparticles tend to aggregate and also have significantly shorter elution lengths than iron microparticles. Under these conditions, the layered column approach described here may actually provide more accurate data about targeting than elution data from mixed sand columns.

ACKNOWLEDGEMENTS

I would like to thank Dr. Tom Mallouk for all of his help, support, and advice over the course of this project. I would also like to thank the members and affiliates of the Mallouk Group, both past and present, for all their assistance at various stages in this project, namely, Emil Hernandez, Tom Larrabee, Brian Kelley, Anna Lee, Camden Henderson, Greg Barber, Joanna Skluzacek, Tiger Wang, John Swierk, Lucas Jellison, Kannan Srinivasan, Yang Wang, Yanyan Cao, and Liz Mack. Particularly, I would like to thank both Laura Hoch for her help and advice orientating me to the project and Liz Seibel for her assistance working on the project. Thanks to Missy Hazen and Ruth Haldeman for help with TEM imaging and to Raafat Mallek for his instruction on zeta-potential measurements. I would also like to thank the John and Elizabeth Holmes Teas program for summer funding. This work was supported by the National Science Foundation under grant CHE-0910513.

WORKS CITED

1. Williams-Johnson, M. M.; Ashizawa, A. E.; De Rosa, C. T. *Human Ecol. Risk Assessment*. **2001,** *7*, 737-753.

2. Mackay, D. M.; Cherry, J. A. *Environ. Sci. Technol*. **1989**, *23*, 630-636.

3. Hoch, L. B.; Mack, E. J.; Hydutsky, B. W.; Hershman, J. M.; Skluzacek, J. M.; Mallouk, T. E. *Eniron. Sci. Technol.* **2008**, *42*, 2600-2605.

4. Suresh, P.; Rao, C.; Annable, M. D.; Sillan, R. K.; Dai, D.; Hatfield, K.; Graham, W. D.; Wood, A. L.; Enfield, C. G. *Water Resour. Res*. **1997**, *33*, 2673-2868.

5. Okuda, I.; McBride, J. F.; Gleyzer, S. N.; Miller, C. T. *Environ. Sci. Technol*. **1996**, *30*, 1852-1860.

6. Slater, G. F.; Lollar, B. S.; Sleep, B. E.; Edwards, E. A. *Environ. Sci. Technol*. **2001**, *35*, 901-907.

7. Rothmel, R. K.; Peters, R. W.; St. Martin, E.; DeFlaun, M. F. *Environ. Sci. Technol*. **1998**, *32*, 1667-1675.

8. Joo, S. H.; Cheng, F. I. *Nanotechnology for Environmental Remediation*, 1st ed.; Springer: New York, 2006; pp 5-12.

9. Li, X.-Q.; Zhang, W.-X. *J. Phys. Chem. C*. **2007**, *111*, 6939-6946.

10. Li, Z. H.; Jones, H.; Bowman, R.; Helferich, R. *Environ. Sci. Technol*. **1999**, *33*, 4326-4330.

11. Cao, J.; Zhang, W.-X. *J. Hazard. Mater*. **2006**, *132*, 213-219.

12. Keum, Y.-S.; Li, Q. X. *Chemosphere*. **2004**, *54*, 255-263.

13. Zhang, W.-X. *J. Nanopart. Res*. **2003**, *5*, 323-332.

14. Zhang, W.-X.; Wang, C.-B.; Lien, H-L. *Catalysis Today*. **1998**, *40*, 387-395.

15. Wang, C.-B.; Zhang, W.-X. *Environ. Sci. Technol*. **1997**, *31*, 2154-2156.

16. Uegami, M.; Kawano, J.; Okita, T.; Fujuu, Y.; Okinaka, K.; Kayuka, K.; Yatagi, S. Iron Particles for Purifying Contaminated Soil or Groundwater. U.S. Patent No. 7,022,256, April 4, 2006.

17. Sahoo, Y.; Goodarzi, A.; Swihard, M. T.; Ohulchanskyy, T. Y.; Kaur, N.; Furlani, E. P.; Prasad, P. N. *J. Phys. Chem. B.* **2005**, *109*, 3879-3885.

18. Hydutsky, B. W.; Mack, E. J.; Beckerman, B. B.; Skluzacek, J. M.; Mallouk, T. E. *Environ. Sci. Technol*. **2007**, *41*, 6418-6424.

19. McNeill, I. C.; Alston, A. *Agnew. Makromol. Chem.* **1998**, *261/262*, 157-172.

20. Idris, S. A.; Mkhatresh, O. A.; Heatley, F. *Polym. Int*. **2006**, *55*, 1040-1048.

21. Luthy, R. G.; Aiken, G. R.; Brusseau, M. L.; Cunningham, S. D.; Gschwend, P. M.; Pignatello, J. J.; Reinhard, M.; Traina, S. J.; Weber, W. J., Jr.; Westall, J. C. *Environ. Sci. Technol.* **1997**, *31*, 3341-3347.

22. Quinn, J.; Geiger, C.; Clausen, C.; Brooks, K.; Coon, C.; O'Hara, S.; Krug, T.; Major, D.; Yoon, W.-S.; Gavaskar, A.; Holdsworth, T. *Environ. Sci. Technol*. **2005**, *39*, 1309-1318.

23. Shrick, B.; Hydutsky, B. W.; Blough, J. L.; Mallouk, T. E. *Chem. Mater*. **2004**, *16*, 2187-2193.

24. Saleh, N.; Phenrat, T.; Sirk, K.; Dufour, B.; Ok, J.; Sarbu, T.; Matyjaszewski, K.; Tilton, R. D.; Lowry, G. D. *Nano Lett*. **2005**, *5*, 2489-2494.

25. Zhan, J.; Zheng, T.; Piringer, G.; Day, C.; McPherson, G. L.; Lu, Y.; Papadopoulos, K.; John, V. T. *Environ. Sci. Technol*. **2008**, *42*, 8871-8876.

26. Saleh, N.; Kim, H.-J.; Phenrat, T.; Matyjaszewski, K.; Tilton, R. D.; Lowry, G. D. *Environ. Sci. Technol*. **2008**, *42*, 3349-3355.

27. Sirk, K. M.; Saleh, N. B.; Phenrat, T.; Kim, H.-J.; Dufour, B.; Ok, J.; Golas, P. L.; Matyjaszewski, K.; Lowry, G. V.; Tilton, R. D. *Environ. Sci. Technol*. **2009**, *43*, 3803-3808.

28. Kralchevsky, P. A.; Nagayama, K. *Adv. Coll. Interf. Sci.* **2000**, *85*, 145-192.

29. Carbonyl Iron Powder – a BASF invention, 2008. BASF Group Web site. http://www.inorganics.basf.com/p02/CAPortal/en_GB/portal/Carbonyleisenpulver_B/content/Produktgruppen/Carbonyleisenpulver/Technologies/Allgemeine_Informationen (accessed Apr 14, 2010).

30. Skoog, D.A.; West, D.M. *Fundamentals of Analytical Chemistry*, 4th ed.; Saunders College Publishing: Philadelphia, PA, 1982; pp 790-791.

31. Dove, J. W.; Buckton, G.; Doherty, C. *Int. J. Pharm*. **1996**, *138*, 199-206.

32. Tufenkji, N.; Elimelech, M. *Environ. Sci. Technol*. **2004**, *38*, 529-539.

33. Mack, E. J. "Targeting of contamination using supported iron particles." The Pennsylvania State University: University Park, PA. Unpublished work, 2006.

34. Hozumi, A.; Asakura, S.; Fuwa, A.; Shirahata, N.; Kameyama, T.; *Langmuir*. **2005**, *21*, 8234-8242.

35. Panzer, J. *J. Coll. Interf. Sci*. **1973**, *44*, 142-161.

36. Mack, E. J.; Fowler, D. E.; Skluzacek, J. M.; Mallouk, T. E. *Chem. Mater*., to be submitted for publication, 2010.

ACADEMIC VITA

Daniel Edward Fowler

Correspondence

Address: 106 Grays Lane
Lansdale, PA 19446

E-mail: def5018@psu.edu
defowl@gmail.com

Education

Major: Chemistry – B.S., Spring 2010, The Pennsylvania State University
Minor: Mathematics
Honors: Phi Beta Kappa; Honors in Chemistry

Thesis
Title: Synthesis of Magnetite-Derived Zero Valent Nanoiron and Targeting of Zero Valent Iron for Application in Environmental Remediation

Supervisor: Dr. Thomas E. Mallouk

Work Experience

Institution: Penn State Department of Chemistry
Title: Research Assistant
Date: March 2008 to May 2010
Supervisor: Dr. Thomas E. Mallouk
Description: Developed a novel green, low-cost synthesis of zero-valent iron to be used to treat groundwater contaminants. Analyzed particles using various characterization techniques (X-ray diffraction, transmission electron microscopy, scanning electron microscopy, UV-Vis spectroscopy, zeta potential). Studied dependence of iron targeting properties on polymer adsorbent properties using sand columns and contact angle measurements. Presented findings at group meeting and at Teas symposium.

Institution: Penn State Department of Chemistry
Title: Teaching Assistant
Date: January 2010 to May 2010
Supervisor: Dr. Jacqueline Bortiatynski
Description: Supervised and instructed a lab section of an introductory organic chemistry class. Introduced students to various chemical separation and purification techniques. Graded various materials and provided students with feedback to improve scientific communication skills. Held office hours to assist students in running instrumentation (NMR, IR, GC, UV-Vis) and interpreting results.

Institution:	Penn State Department of Chemistry
Title:	Exam Proctor and Grader
Date:	January 2008 to December 2009
Supervisor:	Connie Boob
Description:	Monitored students during mid-term and final exams. Directed students on test format and administered tests. Coordinated students during and after test to prevent academic dishonesty. Graded first semester organic chemistry exams.

Institution:	CECO Filters
Title:	Office Assistant
Date:	December 2006 to May 2010
Supervisor:	Pauline Dugas
Description:	Organized electronic and print records of company. Communicated with employees to assist in organization. Used various computer programs (Excel, Tinyterms, Goldmine) to create sales records, literature, memos. Created instruction set and past sales database in current use by company.

Awards and Recognitions

American Chemical Society Undergraduate Inorganic Chemistry Award
Fleming-Meyer Analytical Chemistry Scholarship
John and Elizabeth Holmes Teas Scholarship for Undergraduate Research
John and Elizabeth Holmes Teas Scholarship for Academic Excellence

Presentations

Thesis Defense – April 13, 2010

Community Service Involvement

Penn State Schreyer Honors College SHOTIME Orientation Program Mentor
Penn State Chemistry Department Peer Mentor to Incoming Chemistry Majors
Brookline Retirement Center Volunteer through Penn State Newman Association
Habitat for Humanity Building Volunteer at Georgetown, SC